

Harmonic generation from periodic lattices irradiated by short-pulse laser light

R. Ondarza-Rovira

*Departamento de Física, Instituto Nacional de Investigaciones Nucleares
Apartado postal 18-1027, 11801 México, D. F., Mexico.*

Recibido el 20 de marzo de 1997; aceptado el 22 de agosto de 1997

Radiation emission from thin solid targets irradiated by short-intense laser pulses has been re-examined. Free electrons in the material are driven by the applied external radiation field and harmonics are generated by the electronic response to the crystal lattice force. Recent work on this phenomenon has drawn attention to a flat spectral profile featured by a sudden cut-off at high harmonic order. In the present work we report a number of effects that may in practice have a bearing on the emission. A model was modified by introducing a more general expression for the lattice force that by sharpening or by smoothing the potential in turn allows the strength of the electronic perturbation to be varied. Results from the computed emission reported here show that the pulse shape and the intensity of the laser light may modify the spectral characteristics. For infinite plane waves the obtained emission spectra are in accordance with a recent theoretical model.

Keywords: Laser-solid matter interactions, scattering and emission radiation

La emisión de radiación por blancos metálicos irradiados por pulsos cortos de luz láser intensa ha sido re-estudiada. El campo externo de radiación mueve a los electrones libres a través de un medio con estructura periódica. Los armónicos son generados por la respuesta de los electrones al potencial de la red. Un trabajo teórico reciente sobre este fenómeno ha mostrado perfiles espectrales planos caracterizados por un corte en la región de armónicos de alto orden. En este trabajo reportamos un número de efectos que en la práctica podrían tener injerencia en la emisión de armónicos. Un modelo fue modificado introduciendo una expresión más general para representar los efectos de la red cristalina permitiendo variar la magnitud de la perturbación electrónica. Los cálculos aquí reportados de la emisión muestran que la forma e intensidad del pulso pueden modificar las características espectrales. Para trenes de onda plana infinitas la emisión obtenida es conforme a un reciente modelo teórico.

Descriptores: Interacción laser-sólidos, dispersión y emisión de radiación

PACS: 52.40.Nk; 42.65.Ky; 52.25.Ps

1. Introduction

Recent work on the irradiation of thin solid targets by short-pulse high intensity lasers has drawn attention to the high order of harmonics that can be generated [1]. The model proposed by Hüller and Meyer-ter-Vehn [1] to study harmonic generation from the interaction of laser light with thin film targets describes the mechanism as one in which the electric field of the laser beam drives the free electrons in the solid lattice to large amplitude excursions. Harmonic emission arises from the perturbation produced by the lattice force. Results reported in that work predict that ionized electrons under the action of the periodic lattice potential radiate a spectrum of harmonics characterized by a sharp cut-off which depends on the lattice spacing and the excursion length. This model has been modified, in this work, by introducing a more general expression for the lattice force that by sharpening or by smoothing the potential in turn allows the strength of the perturbation to be varied. For a particular choice of parameters it can be reduced to the model used in Ref. 1.

This mechanism for harmonic generation differs from that involved in harmonic emission from materials illuminated by CO₂ lasers in early experiments by Carman *et al.* [2], where the long laser wavelength provided, for lower input intensities, the conditions for a sufficiently steepened

plasma density profile. The emission was attributed to non-linear resonant absorption with the plasma wave coupling to the radiation field in the steep density gradient and generating harmonics. The spectra in those experiments were distinguished by a sharp cut-off at high harmonic number. This feature led erroneously to identify the cut-off, in a theory proposed by these authors, with that harmonic for which the upper density shelf, characteristic of the steep density profile in these experiments, went underdense and to propose the cut-off as a density diagnostic. This identification was subsequently shown to be incorrect presumably because of the low temporal and spatial resolution used in Carman's calculations.

Recent experimental work [3] that made use of a novel class of lasers known as T^3 (tabletop-terawatt)—that permit high intensities ($\geq 10^{18}$ W/cm²) and short pulses (≤ 1 psec)—showed no cut-off in the emission spectra, as was previously obtained by Gibbon in numerical plasma simulations [4]. Presumably, when external electromagnetic radiation is incident on plasmas characterized by steep density profiles and by plasma frequencies several times critical, density fluctuations on the plasma surface are induced and constitute sources for harmonic generation [5, 6].

The radiation mechanism studied here has features in common with the Smith-Purcell (S-P) effect [7-10] in which

radiation is generated when highly energetic electrons interact with grooves in the surface of a grating. This effect was independently discovered by Salisbury [11]. In this effect coherent radiation is produced from the radio to the ultraviolet spectral region for electrons with energies above 50 keV. The Smith-Purcell effect gives rise to coherent narrow band radiation of frequency $\omega = \mathbf{k}_g \cdot \mathbf{v}(1 - \beta \cos \theta)^{-1}$, where \mathbf{k}_g is the grating periodicity, \mathbf{v} denotes the velocity of a beam electron, $\beta = v/c$ and θ is the angle between the beam direction and the source-observer axis. The last expression can be deduced, as we will see later, from considerations that imply a resonance condition to be fulfilled. The S-P effect offers a means of producing radiation at high efficiency allowing the emission frequencies to be selected by varying the grating period. If electrons strike the surface, the effect could be screened by other mechanisms like transition radiation [12], for example. Experiments have been performed to study the relativistic limit for electrons of energy 3.6 MeV [10] and radiation in the range of 350 μm to 2 mm was detected for grating periods of (0.5–1) mm at emission angles of 56°–150°. The tunability and spatial coherence of the S-P radiation may offer scope for applications in areas such as microscopy and microholography.

Using this idea, the crystal lattice might be regarded as a diffraction grating responsible for the emission when charged particles pass through periodically repeated inhomogeneities—in this case—the equidistant ion cores. The quiver motion of electrons in the non-relativistic limit gives rise to emission at the fundamental frequency ω_L (Thomson scattering).

In this paper we explore, through numerical modeling, the harmonic generation produced when short laser pulses are incident on thin film targets. Emission arises from the electronic response to the lattice potential. We draw attention to the distinct spatial characteristics obtained when effects due to the pulse shape and the intensity of the laser light are introduced in the computations. The remainder of this work is organized as follows: In Sect. 2 we account for the mechanism of harmonic generation by means of a modified theoretical model. Section 3 outlines the dynamic equations used to compute the emission and presents the results, for different laser-target scenarios, from numerical integrations. Finally, we conclude in Sect. 4 by discussing the obtained results.

2. Harmonic generation from periodic arrays

Radiation phenomena from short laser pulses of wavelength $\lambda_L = 1 \mu\text{m}$ interacting with matter have been analysed at intensities from 10^{14} to 10^{17} W/cm². Disintegration effects of the crystalline structure as the laser intensity is risen above certain limit sets a limitation in the maximum amplitude of the input radiation.

The mechanism responsible for harmonic generation from these interactions corresponds to nonlinear effects in the electron quiver motion produced by the periodic lattice

potential. Emission at the fundamental frequency ω_L is produced by non-relativistic electrons whereas the perturbation due to the lattice potential will give rise to harmonics. As it will be seen, the lattice periodicity for harmonic excitation is required in the transversal direction to that of propagation of the laser beam.

The transverse quiver momentum of an electron in the presence of a laser field is given by $\mathbf{p} = m_0 c \mathbf{a}_0$, where $\mathbf{a}_0 = e\mathbf{A}_0/m_0 c^2$ is the normalized (unitless) vector potential of the incident radiation field. Here e , c , m_0 and \mathbf{A}_0 denote the electron charge, the speed of light in vacuum, the electron rest mass and the vector potential, respectively. The laser strength parameter a_0 —the magnitude of the normalized vector potential—is related to the intensity I_L of the field by

$$a_0 \simeq 8.544 \times 10^{-10} I_L^{1/2} (\text{W/cm}^2) \lambda_L (\mu\text{m}),$$

where λ_L is the laser wavelength in microns. From now on the scalar a_0 is used to denote the field strength. Relativistic thresholds ($a_0 \sim 1$) for CO₂ (10.6 μm), Nd (1.06 μm) and Kr-F (0.25 μm) lasers are found for intensities beyond 1.22×10^{16} , 1.22×10^{18} and 2.23×10^{19} W/cm², respectively.

In terms of this parameter the velocity of oscillation is given by $v_{osc} = c a_0 / \gamma_{\perp}$, where $\gamma_{\perp} \simeq (1 + a_0^2)^{1/2}$ is the relativistic factor associated with the transverse electron motion. Under the action of the external electric field the ionized electrons perform large quiver excursions of length $\delta = v_{osc} / \omega_L$. The oscillation amplitude expressed in terms of the parameter a_0 reads

$$\delta = \frac{\lambda_L a_0}{2\pi \gamma_{\perp}}.$$

For instance, an electron driven by a 1 μm laser at an intensity of 10^{15} W/cm² describes excursions of approximately 40 Å and can be perturbed, in an optical cycle, by 20 ion cores in a lattice array with period 4 Å. In addition to this mechanism, the emission produced from the atomic response to the external radiation must be discerned and differentiated from the type of emission we are concerned with.

Atoms exposed to intense laser fields develop time-dependent dipole moments which radiate at odd multiples of the incident frequency. The radiation emitted is associated with the anharmonic motion of bounded atomic electrons. This process, known as optical harmonic generation, is responsible for high order harmonic emission. The electron ionization process can be divided into two regimes. In the first of these, corresponding to low intensities, the ionization occurs when electrons make transitions between bound levels or from atomic levels to the continuum. In those processes harmonic generation is produced. For high field intensities harmonic generation occurs when the electrons pass over the resultant potential barrier of the atomic nucleus and the incident field [13]. In single-atom approximations it has been found that harmonic emission can be reduced when the pulse intensity reaches a threshold value. Beyond that point,

complete ionization takes place and the ionized electrons then emit by bremsstrahlung scattering.

Atomic emission thus corresponds to a process in which electrons experience transitions between different atomic levels before emitting radiation. These processes are characterized by time scales larger than those for the type of emission we are studying here, and this distinction offers a means of discrimination.

At very high laser intensities the crystalline structure might be affected by the action of the radiation field. Distortions to the lattice configuration can then be produced altering the electron harmonic motion through lattice cores. Using ultrashort laser pulses it could be possible to measure the radiation emitted when the interaction time with the driver field is shorter than the disintegration time of a thin solid layer.

To estimate the disintegration time we need to calculate the electron oscillation energy in the field [1], which can be written as

$$E_{osc} \simeq 2.56 \times 10^5 \left(\frac{a_0^2}{1 + a_0^2} \right) \text{ eV}, \quad (1)$$

a parameter that sets the upper limit for the hydrodynamic disintegration velocity $v_{dis} < (E_{osc}/Am_p)^{1/2}$, where A is the mass number of the material and m_p denotes the atomic mass unit. For instance, the disintegration time for a solid layer of thickness 100 Å, $A = 10$ and $E_{osc} \sim 200$ eV—corresponding to a Nd laser with intensity $I_L = 10^{15}$ W/cm²—is $\tau_{dis} > 300$ fs. Thus, for ultrashort laser pulses with time duration below the disintegration time it is possible to ensure that lattice arrays will preserve their periodic structure.

On the other hand, the electrons driven by the electric field have oscillation energies both above the Fermi energy (several electronvolts) and the binding solid energy. For example, for laser intensities greater or equal to $(10^{14}–10^{18})$ W/cm² the electron energies are of the order of $(10–10^5)$ eV.

To account for collisional effects during the excursion of electrons in the material a classical approximation for the collisional cross section can be applied [1]. It can be shown from Eq. (1) that the ratio of the mean free path to the quiver excursion δ is given by

$$\frac{l_{mfp}}{\delta} \sim \frac{3 \times 10^{24}}{n_e \lambda_L} \left(\frac{a_0}{\gamma_{\perp}} \right)^3.$$

From the last equation we see that for solid densities and for laser intensities greater than 10^{14} W/cm² and $\lambda_L = (0.1–10)$ μm, $l_{mfp} > \delta$ and the electrons can make several number of excursions before losing energy between collisions.

The classical equation of motion for free electrons in a solid material under the influence of both a plane monochromatic linearly polarized electromagnetic wave and a lattice potential $\phi(\mathbf{r})$ can be expressed in the form

$$m\ddot{\mathbf{r}}(t) = -e\mathbf{E}_L \sin(\omega_L t - \mathbf{k}_L \cdot \mathbf{r}) + e\nabla\phi(\mathbf{r}). \quad (2)$$

The expression above is only valid for thin layers with skin depths much bigger than the metal thickness under consideration. For thicker layers, the laser field inside the material must be calculated taking account of attenuation factors characteristic of the medium. For those situations the laser electric field assumes the form

$$E = E_0 e^{-\frac{\omega_L}{c} n \kappa x} \cos \omega_L \left(\frac{n}{c} x - t \right),$$

with attenuation determined by the exponential term. Here n is the refraction index and $n^2 \kappa = 2\pi\mu\sigma/\omega_L$, where μ and σ are the permeability and conductivity of the medium, respectively; κ is called the attenuation index. Since the energy density \mathcal{E} of the wave is proportional to the time average of E^2 , \mathcal{E} decreases as $\mathcal{E} = \mathcal{E}_0 e^{-\chi x}$, where $\chi = 2\omega_L n \kappa / c$ is the absorption coefficient. The energy density decays to $1/e$ after the wave has travelled over a distance $d = 1/\chi = \lambda_L / 4\pi\kappa n$, the skin depth.

Essentially, the electron trajectories consist of harmonic oscillations $\mathbf{r}(t) = \mathbf{r}_0 + \mathbf{r}_1(t) + \mathbf{r}_2(t)$, around centres \mathbf{r}_0 , where $\mathbf{r}_1(t) = \delta \sin(\omega_L t - \mathbf{k}_L \cdot \mathbf{r}_0)$ is the quiver electron motion with amplitude $\delta = e\mathbf{E}_L / m\omega_L^2$ and $\mathbf{r}_2(t)$ corresponds to small deviations produced by the perturbation of the lattice force.

With the aim of representing the periodic lattice force acting on electrons as they make excursions through the crystalline array we considered a potential $\phi(\mathbf{r})$ of the form

$$\phi(\mathbf{r}) = \sum_c \phi_c \sinh [A \sin(\mathbf{k}_c \cdot \mathbf{r})], \quad (3)$$

where $\mathbf{k}_c = k_c \hat{\mathbf{e}}_c$ corresponds to the reciprocal lattice vectors and the strength amplitude ϕ_c is of the order of one volt for typical metals [15]. The factor A in the last expression can be incorporated into the model in order to include variations in the lattice potential. The lattice potential considered in Eq. (3) can be reduced to the sinusoidal potential conventionally used for representing periodic potentials and applied by Hüller and Meyer-ter-Vehn in Ref. 1. Some plots for this function, normalized to unity, are shown in Figs. 1a and 1b, where variations to the sinusoidal form were produced by assigning different values to the parameter A .

Following Hüller and Meyer-ter-Vehn's model and incorporating a more general expression for the lattice potential, as considered above, the lattice force gives rise to a perturbed motion described by

$$m\ddot{\mathbf{r}}_2 \sim - \sum_c eA \phi_c \mathbf{k}_c \cos(\mathbf{k}_c \cdot \mathbf{r}) \cosh[A \sin(\mathbf{k}_c \cdot \mathbf{r})].$$

Using Jacobi expansions for the arguments one can get the corresponding expressions for the sin and cos terms

$$\sin(\mathbf{k}_c \cdot \mathbf{r}) = \sum_m \epsilon_m J_m(Z) \cos(m\theta') \sin\left[\frac{m\pi}{2} + \mathbf{k}_c \cdot \mathbf{r}_0\right],$$

$$\cos(\mathbf{k}_c \cdot \mathbf{r}) = \sum_m \epsilon_m J_m(Z) \cos(m\theta') \cos\left[\frac{m\pi}{2} + \mathbf{k}_c \cdot \mathbf{r}_0\right],$$

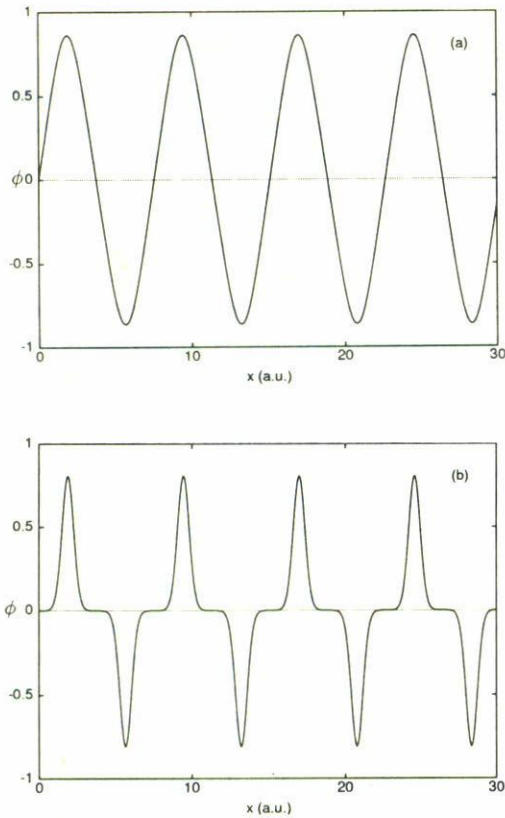


FIGURE 1. Lattice potential as represented by Eq. (3) for arbitrary values of A .

where ϵ_m is the Neumann parameter defined by $\epsilon_m = 1$ for $m = 0$ and $\epsilon_m = 2$ for $m \neq 0$, $\theta' = \pi/2 - \theta$, $Z = \mathbf{k}_c \cdot \boldsymbol{\delta}$ and $\theta = \omega_L t + k_L \boldsymbol{\Omega} \cdot \mathbf{r}_0 - \omega_L c \boldsymbol{\Omega} \cdot \mathbf{R}_{\text{obs}}$. Here \mathbf{R}_{obs} is the vector to the observation point and $\boldsymbol{\Omega}$ a unit vector from the particle to the observer.

Harmonics are generated due to the lattice force $m \ddot{\mathbf{r}}_2(t')$, evaluated at the retarded time $t' = t - \boldsymbol{\Omega} \cdot (\mathbf{R}_{\text{obs}} - \mathbf{r})/c$. In what follows, the prime has been dropped for convenience.

Hence, the acceleration is given by

$$\ddot{\mathbf{r}}_2 \sim - \sum_c \frac{e}{m} \phi_c \mathbf{k}_c A \sum_m \epsilon_m J_m(Z) \cos \alpha(t) \cos \beta \times \cosh \left[A \sum_m \epsilon_m J_m(Z) \cos \alpha(t) \sin \beta \right], \quad (4)$$

where

$$\alpha(t) = \frac{1}{2} m \pi - \omega_L t + b,$$

$$\beta = \frac{1}{2} m \pi + (\mathbf{k}_c \cdot \mathbf{r}_0),$$

$$Z = (\mathbf{k}_c \cdot \boldsymbol{\delta}),$$

$$b = k_L \boldsymbol{\Omega} \cdot \mathbf{r} - \mathbf{k}_L \cdot \mathbf{r}_0 - \frac{\omega_L}{c} \boldsymbol{\Omega} \cdot \mathbf{R}_{\text{obs}}.$$

The power radiated by single electrons per unit solid angle in the direction $\boldsymbol{\Omega}$ is given by [14]

$$\frac{dP(t)}{d\Omega} = \frac{c}{4\pi} |R \mathbf{E}_{\text{rad}}(t, \boldsymbol{\Omega})|^2,$$

where

$$\mathbf{E}_{\text{rad}}(t, \boldsymbol{\Omega}) = - \frac{e}{c^2} \frac{\boldsymbol{\Omega} \times (\boldsymbol{\Omega} \times \ddot{\mathbf{r}}(t'))}{R},$$

and $R = |\mathbf{R}_{\text{obs}} - \mathbf{r}|$.

The spectral components are then obtained by evaluating and Fourier analysing the acceleration field. The emission calculated by means of this procedure is in accordance with that obtained by integrating numerically the electron force equation, step we follow in next section. The lattice force as a function of time is also shown for different intensities.

In order to have an insight into the maximum harmonic number that can be generated from the action of the lattice force on the electron motion we follow a procedure that involves conservation of energy and momentum.

The radiation spectrum produced when a charged particle moves in the vicinity of a periodic structure can be explained from conservation laws. Radiation arises only if resonance conditions are fulfilled. To explain the last statement, let us assume that the medium changes its properties periodically along a certain direction y . If we consider a particle travelling through a medium with velocity v emitting quanta of energy $\hbar\omega$ and momentum $\hbar\omega/c$, the conservation laws for the longitudinal momentum and the energy can be written in general form as

$$\frac{v \delta \mathbf{p}}{v} - \frac{\hbar\omega}{c} \cos \theta' = \frac{2\pi}{l} m, \\ \delta E - \hbar\omega = 0,$$

where θ' is the angle between the direction of a quantum emitted and the velocity \mathbf{v} . The changes in energy and momentum of the particle are denoted by δE and $\delta \mathbf{p}$ respectively, m is an arbitrary integer and l the periodicity of the medium. Since $\delta E = v \delta \mathbf{p}$ for small changes of the energy of the particle, the principal condition for radiation from the conservation laws reads

$$\frac{\omega_{\text{eff}}}{v} = \frac{\omega}{v} \left(1 - \frac{v}{c} \cos \theta' \right) = \frac{2\pi m}{l}.$$

For the finite plane wave-solid interaction, the spectrum forms a plateau in the region of low harmonic orders with a cut-off near the peak intensity. The location of the cut-off can then be derived from the resonance condition $n_{\text{max}} \omega_L \sim k_c v_{\text{osc}}$, which yields

$$n_{\text{max}} \simeq \left(\frac{\lambda_L}{l_c} \right) \frac{a_0}{\gamma_{\perp}}, \quad (5)$$

where l_c is the lattice spacing.

The overall strength of the spectrum is determined by the electron distribution. From the analysis of the phase factors involved in the expression for the acceleration field it can be shown that correlations between electrons are important [1],

in the sense that for cases in which the electrons are correlated the radiation emitted will be enhanced and at the same time will produce only harmonics of odd order. For disordered electron systems, the emission is found to be less intense and harmonics of any order are permitted. The former case—which represents a more realistic electron behavior—would correspond to oscillation centres that cluster at the sites of the ions or at interstitial locations.

3. Integration of the equation of motion

In spite of the fact that the model outlined above is restricted to low laser intensities, we have adopted it to solve the electron dynamics using a relativistic description, which allows effects that arise for relatively high laser powers to be included. In order to study the dynamics of electrons in the radiation field, a single-particle relativistic force equation for a linearly polarized electromagnetic plane wave with a lattice force term as an external source was solved in order to incorporate nonlinear and quasi relativistic effects that arise when the laser intensity increases to high values.

The electron dynamics was obtained through the numerical solution of the Lorentz equation

$$\frac{d\mathbf{p}}{dt} = -e\mathbf{E} - \frac{e}{c}\mathbf{v} \times \mathbf{B} + e\nabla\phi, \quad (6)$$

where the electromagnetic fields are related to the vector potential in the form

$$\mathbf{E} = -\frac{1}{c}\frac{\partial\mathbf{A}}{\partial t}; \quad \mathbf{B} = \nabla \times \mathbf{A},$$

and ϕ denotes the lattice potential as given by Eq. (3). We have considered a lattice close in shape to the conventional potential, depicted in Fig. 1a. Variations of the lattice potential and its rôle in harmonic generation will be consider in a future publication.

For a monochromatic plane wave of arbitrary polarization propagating along the x direction, the vector potential can be expressed as

$$\mathbf{A}(\mathbf{r}, t) = a(\eta)\mathbf{A}(\eta),$$

where $a(\eta)$ is a shape factor, and

$$\mathbf{A}(\eta) = \left[0, \delta \cos \eta, (1 - \delta^2)^{1/2} \sin \eta \right],$$

here $\eta = w_L(t - x/c)$ is the Lorentz invariant phase. The propagation is taken in the direction of the Poynting vector. The parameter δ characterizes the degree of elliptic polarization. Linear polarization corresponds to $\delta = 0, \pm 1$ and circular polarization to $\delta = \pm 1/\sqrt{2}$.

Using the expression for the electromagnetic potential, as well as the gauge fields equations, the components of the

force equation take the form

$$\dot{v}_x = -\frac{e\omega_L}{mc^2\gamma} \left(1 - \frac{v_x}{c} \right) \left(v_y \frac{dA_y}{d\eta} + v_z \frac{dA_z}{d\eta} \right) + F_p^x, \quad (7)$$

$$\dot{v}_y = -\frac{e\omega_L}{mc\gamma} \left(1 - \frac{v_x}{c} - \frac{v_y^2}{c^2} \right) \frac{dA_y}{d\eta} + \frac{e\omega_L}{mc^3\gamma} v_y v_z \frac{dA_z}{d\eta} + F_p^y, \quad (8)$$

$$\dot{v}_z = -\frac{e\omega_L}{mc\gamma} \left(1 - \frac{v_x}{c} - \frac{v_z^2}{c^2} \right) \frac{dA_z}{d\eta} + \frac{e\omega_L}{mc^3\gamma} v_y v_z \frac{dA_y}{d\eta} + F_p^z, \quad (9)$$

where γ is the relativistic factor given by $\gamma = (1 - \beta^2)^{-1/2}$ and $\beta = |\mathbf{v}|/c$. Here, $F_p^i (i = x, y, z)$ stands for the components of the lattice force, given by

$$F_p^x = -\frac{e}{m\gamma} \left[\left(1 - \frac{v_x^2}{c^2} \right) (\nabla\phi)_x - \frac{v_x v_y}{c^2} (\nabla\phi)_y \right], \quad (10)$$

$$F_p^y = -\frac{e}{m\gamma} \left[\left(1 - \frac{v_y^2}{c^2} \right) (\nabla\phi)_y - \frac{v_y v_x}{c^2} (\nabla\phi)_x \right], \quad (11)$$

$$F_p^z = \frac{ev_z}{mc^2\gamma} \left[v_x (\nabla\phi)_x + v_y (\nabla\phi)_y \right]. \quad (12)$$

For linear polarization, which is the case of interest for us in this calculation to obtain the emission from the quiver electron motion, one can consider the electric field directed along the y cartesian axis, and by setting δ equal to unity it results in

$$E_y = -\frac{w_L}{c} \left[\frac{\partial a(\eta)}{\partial \eta} \cos \eta - a(\eta) \sin \eta \right].$$

In any model of short-pulse irradiation of targets it is clearly important to take account of the pulse shape $a(\eta)$, which we have incorporated as a gaussian envelope of the form

$$a(\eta) = a_0 e^{-\alpha(\eta - \eta_0)^2},$$

where a_0 gives the strength of the field and α the width of the envelope.

An equation that approximates the acceleration force on the electrons during their excursions through the atomic potential can be written in a short form by considering only the first term on the right hand side of Eq. (11), since for the laser intensity regime we are considering, contributions of the lattice potential along the direction of propagation of the wave can be neglected. In fact, for a laser intensity of $I = 10^{15}$ W/cm² the electron displacement in the forward direction during a laser period is approximately $\delta_x/l_c = 0.5$. We can then represent this force by the expression

$$\delta\dot{v}_y = \frac{e}{m} \sqrt{1 - \beta^2} \phi_c k_c \sin(k_c y) \left(1 - \frac{v_y^2}{c^2} \right).$$

With the aim of verifying the numerical integration of the force equations during the pulse duration we have applied the

conservation of energy which can be expressed in terms of the electron velocities in the form

$$\frac{\gamma^3}{c^2} \sum_i v_i v_i = \frac{e}{mc^2} \sum_i v_i [E_i + (\nabla\phi)_i],$$

where the index i denotes the spatial coordinates x, y and z .

The electron trajectories represent harmonic oscillations with large amplitudes proportional to the electric field. The electric field of the laser beam causes the electrons to oscillate at the fundamental frequency, and as the intensity increases the electron motion develops higher harmonic components due to the nonlinear lattice interaction. Different graphs representing the lattice force as a function of time were obtained. The numerical integration performed here was carried out using atomic units, in which $e = m = \hbar = 1$ and $c = 137.07$. In this metric the most used units are given as $1 \text{ gr} = 1.098 \times 10^{27} \text{ a.u.}$, $1 \text{ cm/sec} = 4.572 \times 10^{-9} \text{ a.u.}$, $1 \text{ sec} = 4.132 \times 10^{16} \text{ a.u.}$, $1 \text{ cm} = 1.889 \times 10^8 \text{ a.u.}$, $1 \text{ V/cm} = 1.945 \times 10^{-10} \text{ a.u.}$ and $1 \text{ W} = 5.554 \text{ a.u.}$

The procedure discussed here reproduces the emission spectrum with the plateau and the cut-off obtained by Hüller and Meyer-ter-Vehn [1] for a thin solid layer illuminated by a subpicosecond laser pulse. The cut-offs were also found at the predicted values n_{max} , as given by Eq. (5). In what follows, we describe some results obtained from numerical calculations.

We have considered a number of cases including top-hat profiles and gaussians of different half-widths. In the following we present some radiation spectra obtained from the perturbed electron motion. Figs. 2–6 show some results for an infinite plane wave incident on target.

Figure 2a shows the lattice force as a function of $t' = \omega_L t / \pi$ for an electron perturbed by the potential described by Eq. (3). The lattice period is taken as $l_c = 4 \text{ \AA}$, the laser intensity as $I_L = 10^{14} \text{ W/cm}^2$ and the laser wavelength as $\lambda_L = 1 \mu\text{m}$. The electrons oscillate with amplitude $\delta = 14 \text{ \AA}$ and experience an additional acceleration produced by 13 lattice cores during one optical cycle. This graph shows the lattice acceleration and deceleration of electrons as they perform excursions through the solid layer. The wider peaks correspond to turning points where electrons complete half their oscillation. Figure 2b shows the emission for this motion. For this low intensity, the cut-off is found to be at $n = 22$ which is in accordance with the analytic prediction given by Eq. (5). The spectrum is normalized by a factor $f_n = 6.5 \times 10^{-4}$ and where the emission at the fundamental frequency has been removed.

For an intensity of $I_L = 10^{15} \text{ W/cm}^2$ Figs. 3a and 3b show the electron acceleration and the radiation emitted, respectively. For this case, the electron traverses through 40 lattice sites and the radiation spectrum forms a well-defined plateau with a cut-off located around $n = 71$, as predicted again by expression (5). The peak intensity is near the cut-off value and in this case $f_n = 1.27 \times 10^{-5}$.

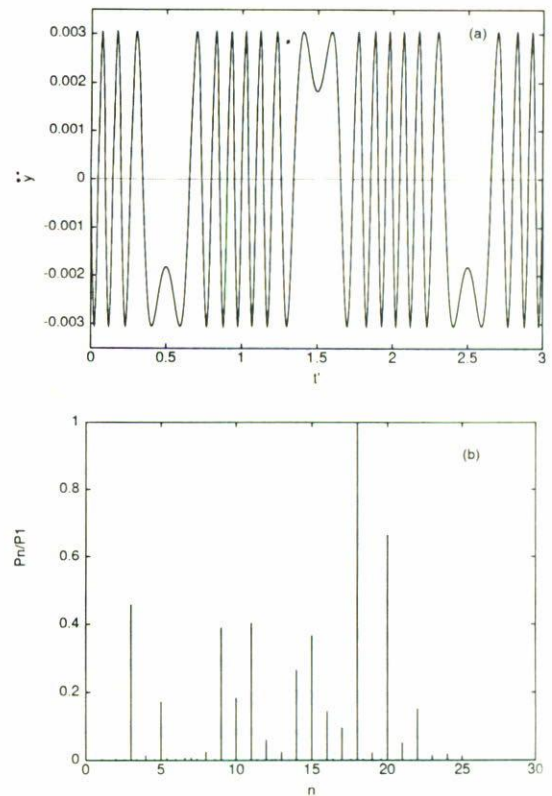


FIGURE 2. a) Lattice force vs. $t' = \omega_L t / \pi$. $I_L = 10^{14} \text{ W/cm}^2$, $\lambda_L = 1 \mu\text{m}$ and $l_c = 4 \text{ \AA}$. b) Radiation spectrum.

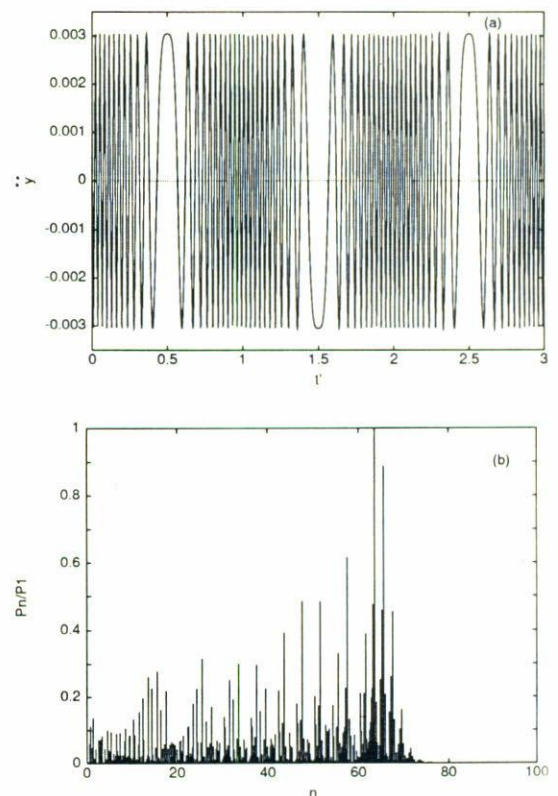


FIGURE 3. a) Lattice force vs. $t' = \omega_L t / \pi$. $I_L = 10^{15} \text{ W/cm}^2$, $\lambda_L = 1 \mu\text{m}$ and $l_c = 4 \text{ \AA}$. b) Radiation spectrum.

Figures 4a and 4b correspond to the case $I_L = 10^{16} \text{ W/cm}^2$. Here the electron acceleration is greater than in previous cases and the spectrum is characterized as well by a plateau with a sharp peak near the cut-off. Values are normalized according to $f_n = 1.0 \times 10^{-6}$. In this case, the cut-off is at $n = 220$.

In the plot shown in Fig. 5a the harmonic numbers corresponding to the peak intensities for the plane wave-solid interaction are sketched as a function of laser intensity. Although the high order emission might be resolved experimentally, it is of particular interest that the emission grows parabolically with laser intensity.

Figure 5b displays the power for the highest harmonic number produced as a function of intensity. Here is evident that as the driver intensity rises the generation of harmonics increases but with lower energy. This can be explained in terms of the energy distribution that decays from the fundamental order to the high order region. This figure shows that the decrease with intensity of harmonic amplitudes scales approximately as $I_L^{-1/6}$. No theory, until now, has corroborated this scaling.

In Fig. 6a total power for the overall production is plotted as a function of intensity. From this graph, it is clear that the power emitted increases with input energy.

At an intensity of 10^{15} W/cm^2 Fig. 6b shows the maximum harmonic order produced for different laser wavelengths. As expected, the larger the laser wavelength the

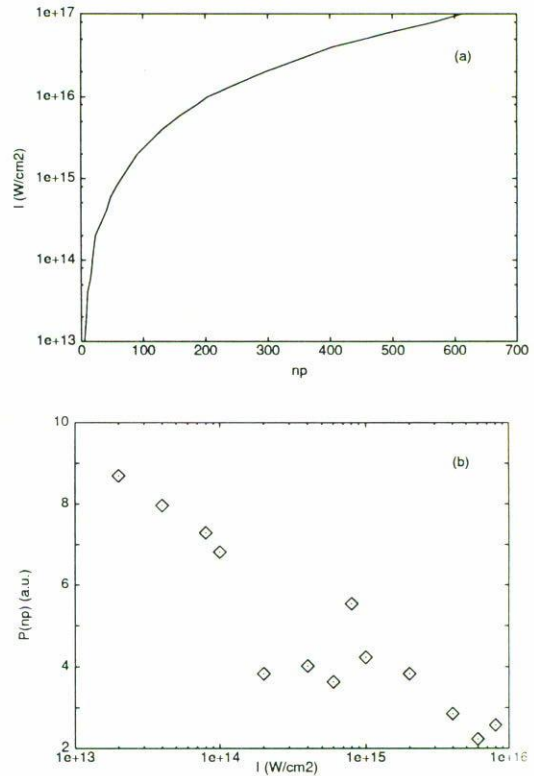


FIGURE 5. a) Laser intensity vs. peak harmonic numbers. b) Power of the highest harmonic number produced vs. intensity, $\lambda_L = 1 \mu\text{m}$ and $l_c = 4 \text{ \AA}$.

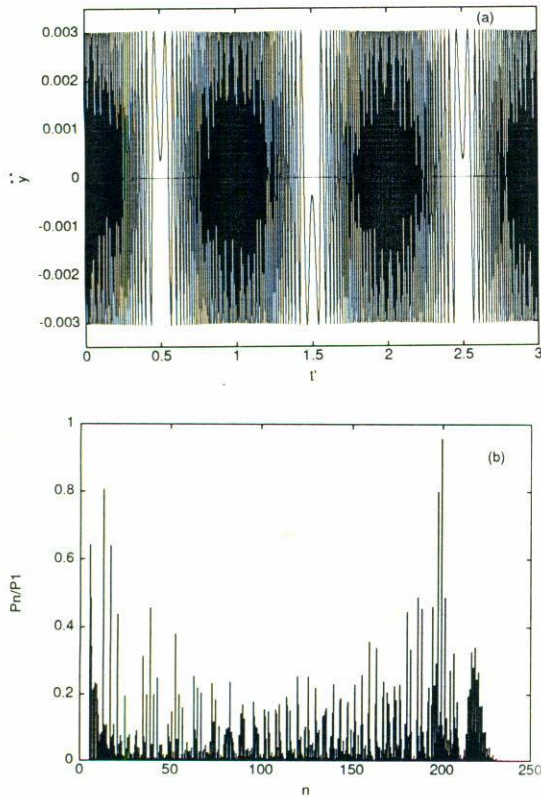


FIGURE 4. a) Lattice force vs. $t' = w_L t / \pi$. $I_L = 10^{16} \text{ W/cm}^2$, $\lambda_L = 1 \mu\text{m}$ and $l_c = 4 \text{ \AA}$. b) Radiation spectrum.

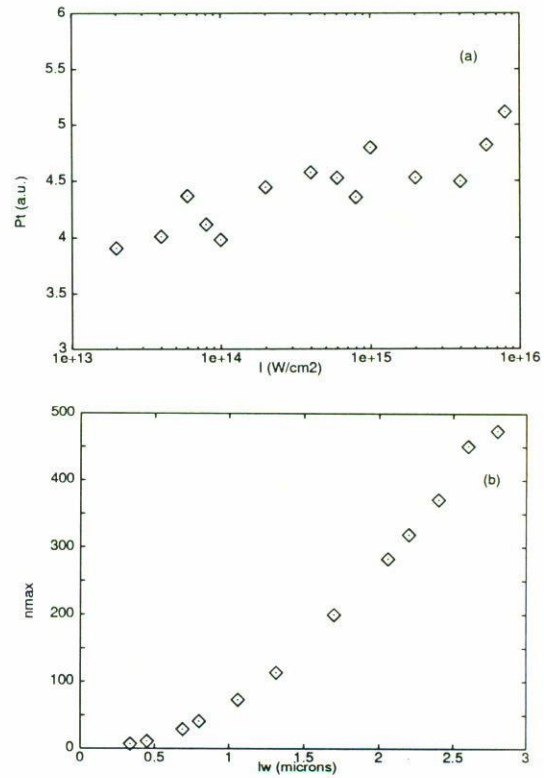


FIGURE 6. a) Total power emitted vs. intensity, $\lambda_L = 1 \mu\text{m}$ and $l_c = 4 \text{ \AA}$. b) Cut-off harmonic number vs. laser wavelength, $I_L = 10^{15} \text{ W/cm}^2$.

higher the harmonic number produced. The wavelengths used in this figure correspond to Dye ($\lambda = 0.3\text{--}1.1\ \mu\text{m}$), Ti:Sapphire ($\lambda = 0.7\text{--}0.9\ \mu\text{m}$), Nd-glass ($\lambda = 1.06\ \mu\text{m}$), Iodine ($\lambda = 1.32\ \mu\text{m}$), Holmium ($\lambda = 2.06\ \mu\text{m}$) and Color centre ($\lambda = 1\text{--}4\ \mu\text{m}$) lasers.

With the purpose of studying a more realistic laser-solid interaction, envelope functions of gaussian type were used for the vector potential that describes the electromagnetic laser fields. Different graphs from these analyses are shown for several pulse durations and were modulated by envelope functions as the one shown by Fig. 7a. In Fig. 7b the emission is shown. The duration of the pulse for this case is of the order of $180\ \text{fs}$ and $f_n = 1.8 \times 10^{-6}$.

Figure 8a corresponds to a gaussian-like pulse of duration $90\ \text{fs}$. The emission for this case is depicted in Fig. 8b, where $f_n = 6.0 \times 10^{-6}$.

Finally, Fig. 9a shows the electric field modulated by a gaussian envelope. The emission is shown in Fig. 9b, here $f_n = 1.5 \times 10^{-5}$.

For completeness, we analyse the dynamics of single free electrons inside a lattice in the presence of an external radiation field modulated by an arbitrary profile. The lattice potential, as treated here, represents a small perturbation in the dynamics and for the cases studied there were no significant deviations in the electron trajectories as compared to the unperturbed case. The electron dynamics for linearly polar-

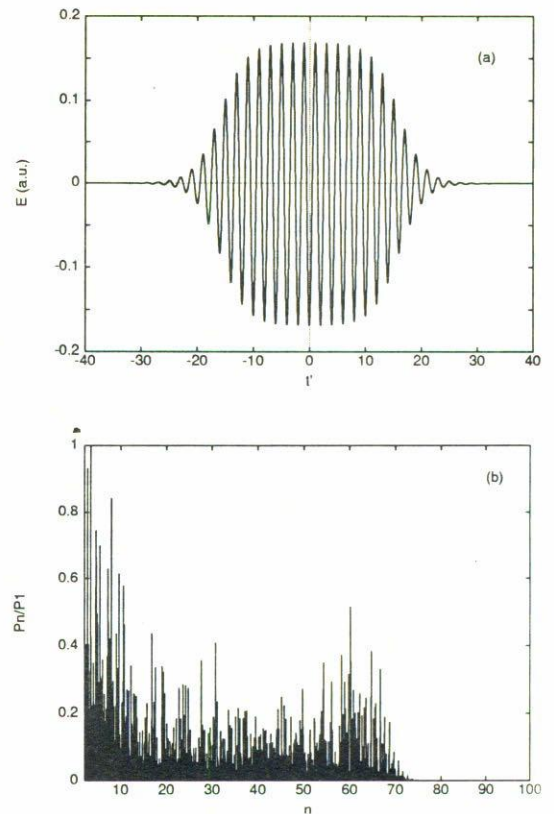


FIGURE 8. a) Laser electric field vs. $t' = \omega_L t / \pi$. $I_L = 10^{15}\ \text{W/cm}^2$, $\lambda_L = 1\ \mu\text{m}$ and $l_c = 4\ \text{\AA}$. b) Radiation spectrum.

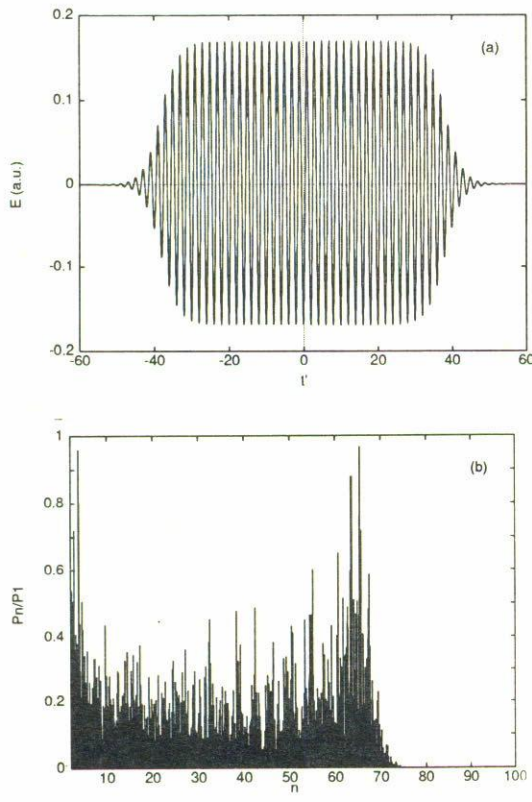


FIGURE 7. a) Laser electric field vs. $t' = \omega_L t / \pi$. $I_L = 10^{15}\ \text{W/cm}^2$, $\lambda_L = 1\ \mu\text{m}$ and $l_c = 4\ \text{\AA}$. b) Radiation spectrum.

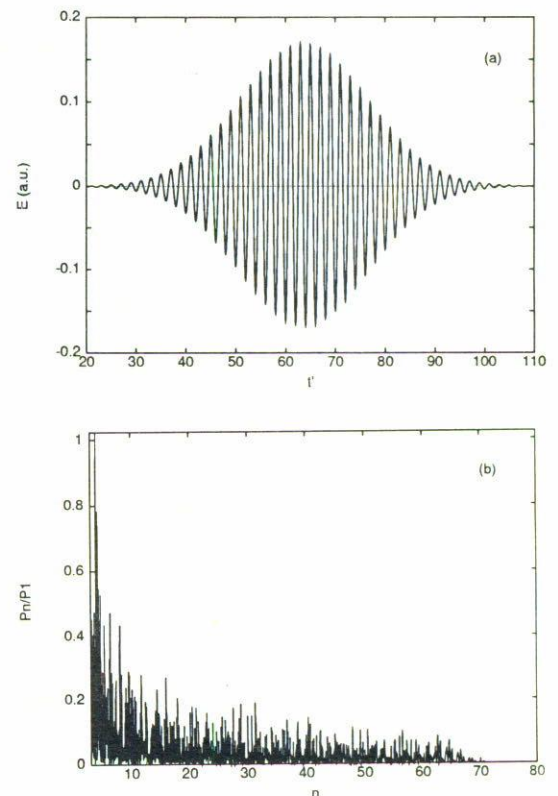


FIGURE 9. a) Laser electric field vs. $t' = \omega_L t / \pi$. $I_L = 10^{15}\ \text{W/cm}^2$, $\lambda_L = 1\ \mu\text{m}$ and $l_c = 4\ \text{\AA}$. b) Radiation spectrum.

ized waves can be solved analytically for arbitrary pulse shapes, in both classical and quantum mechanics. Solutions to this problem were provided by Sarachik and Schapert [16] in a classical theory based on a Hamilton-Jacobi scheme. Krüger and Bovyn [17] analysed the relativistic motion of charged particles in a plane-wave electromagnetic field with arbitrary amplitude, as a generalization of previous work by Sanderson [18].

The free electrons are considered to be at rest prior to the arrival of the laser pulse, and return to that state after the passage of the external field. In general, according to different situations—as those for initial conditions—electrons may not return to their rest state. Similar situations were analysed numerically by Bardsley *et al.* [19] with the inclusion of the plasma response, associated with space charge forces for high plasma densities. In their analyses, strong residual momenta were acquired by the electrons after the electromagnetic interaction for certain threshold values of the plasma frequency. For the present analysis, the introduction of the lattice potential in the force equations did not show the appearance of residual momenta.

The electron dynamics is shown in the following figures, from Figs. 10 to 12. For the case of a laser pulse duration of the order of 200 fs, peak intensity of $I_L = 10^{15}$ W/cm² and $\lambda_L = 1$ μ m, Fig. 10a shows the electron displacement in the direction of propagation of the wave. It also shows that electrons return to rest after the interaction. The time is scaled as $w_L t/\pi$. Figure 10b shows the corresponding electric field,

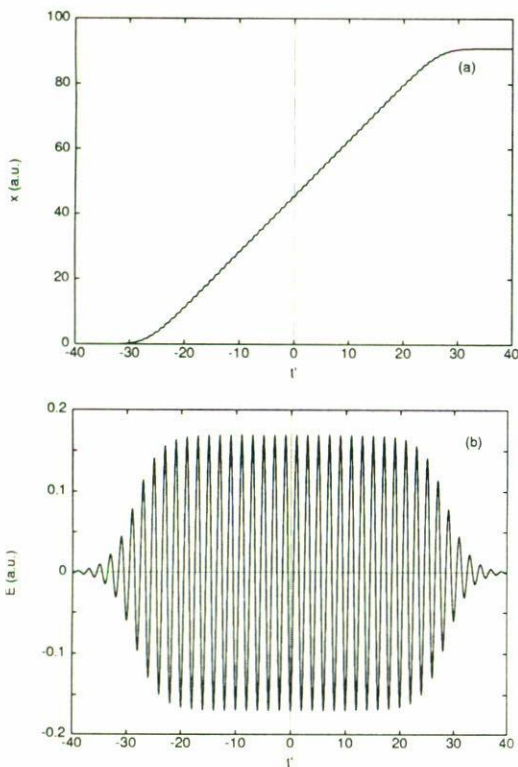


FIGURE 10. a) x drift vs. $t' = w_L t/\pi$. b) Laser electric field vs. $t' = w_L t/\pi$. $I_L = 10^{15}$ W/cm², $\lambda_L = 1$ μ m.

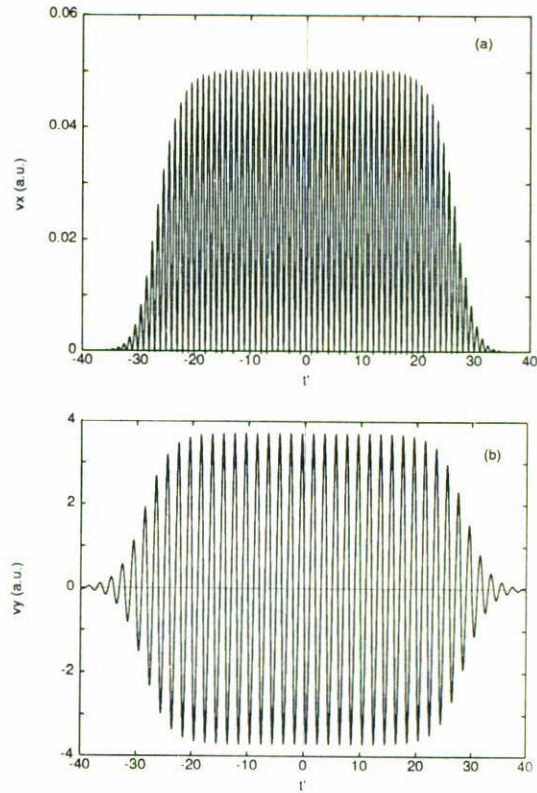


FIGURE 11. a) v_x vs. $t' = w_L t/\pi$. b) v_y vs. $t' = w_L t/\pi$. $I_L = 10^{15}$ W/cm², $\lambda_L = 1$ μ m.

while Figs. 11a and 11b show respectively, as a function of time, the electron velocities in the parallel and perpendicular direction to the wave propagation.

Finally, Figs. 12a and 12b sketch the electron phase space for the velocities and for the accelerations, respectively.

4. Conclusions

Optical harmonic spectra from the electron motion driven by a laser field and under the influence of a periodic lattice potential were obtained.

It was found that the maximum harmonic number emitted from these interactions was located at the cut-off in the spectra and is in accordance with those values predicted by the perturbation model outlined in Ref. 1. It was also shown that the emission power depends strongly on input intensity. For high intensities the cut-off is localized at large harmonic numbers, but at the same time the strength of the emission for the highest harmonic numbers is considerably reduced. This fact is reminiscent of emission processes in single electron-atom interactions, where high intensity laser pulses do not necessarily increase the harmonic production rate. Energy is then distributed among the lower harmonic orders near the fundamental frequency leaving less for the rest of the emission.

Another feature that emerged from computed emission was that the spectra changed significantly from the plateau-cut-off configuration when the external electric field was

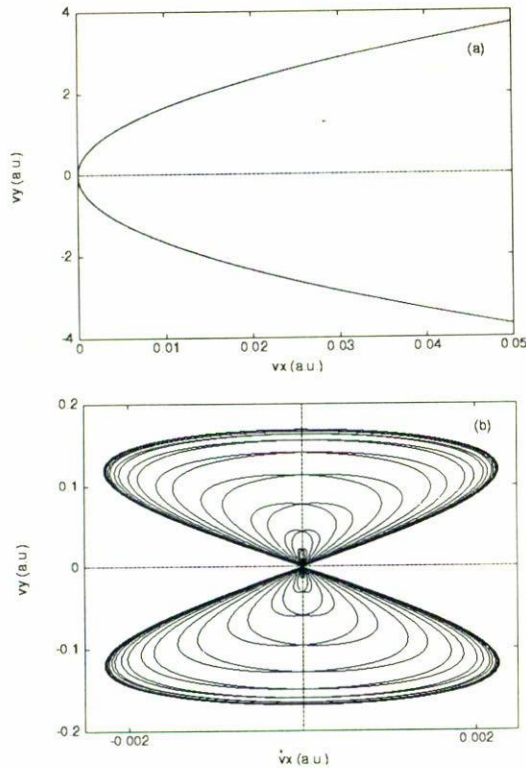


FIGURE 12. a) v_x vs. v_y . b) \dot{v}_x vs. \dot{v}_y . $I_L = 10^{15}$ W/cm², $\lambda_L = 1 \mu\text{m}$.

modulated by different envelopes. In particular, for gaussian pulses, the strongest emission was found to be emitted by lower harmonic numbers and a cut-off was still observed and localized around the value which corresponds to the peak laser electric field during the pulse. From the examples presented along with a sensitivity to the magnitude and form of the lattice potential we conclude that each of these effects will affect the spectral characteristics.

The cut-off in the vacuum-UV or, for higher incident intensities, in the soft X-ray region, provides the most distinctive signature of the emission and, if detected, might hold some potential as a diagnostic.

A possible application of harmonic light emitted from the mechanism discussed here is that it could be used to determine the structure characteristics of irradiated targets.

All in all it seems likely that interpretation and study of spectra from the effect identified by Hüller and Meyer-ter-Vehn would be challenging.

Acknowledgments

The author gratefully acknowledges the guidance and useful conversations with Prof. T.J.M. Boyd, which contributed for the preparation of this work. This work was performed under the auspices of CONACyT.

1. S. Hüller and J. Meyer-ter-Vehn, *Phys. Rev. A* **48** (1993) 3906.
2. R.L. Carman, C.K. Rhodes, and R.F. Benjamin, *Phys. Rev. A* **24** (1981) 2649.
3. P.A. Norreys *et al.*, *Phys. Rev. Lett.* **76** (1996) 1832.
4. P. Gibbon, *Phys. Rev. Lett.* **76** (1996) 50.
5. R. Lichters, *et al.*, *Phys. Plasmas* **3** (1996) 3425.
6. T.J.M. Boyd and R. Ondarza, in *Proceedings of the 1996 Int. Conf. on Plasma Physics*, edited by H. Sugai and T. Hayashi, Vol. 2, (Nagoya, 1996), p. 1718.
7. S.J. Smith and E.M. Purcell, *Phys. Rev.* **92** (1953) 1069.
8. M.J. Moran, *Phys. Rev. Lett.* **69** (1992) 2523.
9. G. Doucas *et al.*, *Phys. Rev. Lett.* **69** (1992) 1761.
10. G. Doucas *et al.*, *Nuclear Inst. & Methods A* **331** (1993) 609.
11. W. Salisbury, *US Patent No.* 2634372 (1953).
12. V.L. Ginzburg and I.M. Frank, *Zh. Eksp. Teor.* **16** (1946) 15.
13. V.C. Reed and K. Burnett, *Phys. Rev. A* **46** (1992) 424.
14. J.D. Jackson, *Classical Electrodynamics*, (John Wiley & Sons, New York, 1962).
15. D.G. Pettifor, in *Physical Metallurgy*, edited by R.W. Cahn and P. Haasen, (North-Holland, Amsterdam, 1983).
16. E.S. Sarachik and G.T. Schappert, *Phys. Rev. D* **1** (1970) 2738.
17. J. Krüger and M. Bovyn, *J. Phys. A: Math. Gen.* **9** (1976) 1841.
18. J.J. Sanderson, *Phys. Lett.* **18** (1965) 114.
19. J.N. Bardsley, B.M. Penetrante, and M.H. Mittleman, *Phys. Rev. A* **40** (1989) 3823.